8.8

ON STRONG DEPENDENCE OF BEHAVIOR OF A NUMERICALLY-SIMULATED CLASSIC SUPERCELL ON GRID SIZE

Akira NODA* and Hiroshi NIINO
The Ocean Research Institute, University of Tokyo

1 INTRODUCTION

Progress in the computer technology now allows us to simulate meso α- or β-scale precipitation system with much fine horizontal resolution of $2 \sim 5$ km (e.g., Yanase et al. 2001). In such simulations, γ-scale cumulus convections which develop in the parent system are often assumed to be resolved explicitly, and no cumulus parameterization is used. However, it is not clear to what extent numerical model with $2 \sim 5$ km grid size resolves individual cumulus convections.

Some studies examined the sensitivity of the meso β-scale precipitation system such as a squall line to the grid size (e.g., Weisman et al. 1997), however, few studies have attempted to investigate a single convective cloud on grid size. Recently, Adlerman and Droegemeier (2001) examined the dependence of the Del City supercell storm on grid size as well as physical processes, and showed that the cyclic generation of the mesocyclone is significantly affected by the model resolution.

Numerical prediction of hazardous convective storms which cause torrential rain and strong wind is becoming more and more important. Thus, it seems necessary to understand what resolution is needed to express such convective storms. In this study, we focus on a supercell, whose basic evolution is relatively understood, and study dependence of its behavior on grid size.

2 NUMERICAL MODEL

The three-dimensional model of the compressible atmosphere used in the present study is ARPS Version 4.5.1 (Xue et al., 1995). In order to examine sensitivity of the simulated convective cloud to the horizontal resolution in the model, we performed the experiments in which the horizontal grid size is varied from 1.0 km to 3.0 km with 0.1 km interval. Hereafter, a simulation with a horizontal grid size of x km is referred to as x km-run.

To make sure that the sensitivity only to the horizontal grid size is studied, all of the other conditions are kept same. The calculation domain is nearly 127 km $\times$ 127 km in the horizontal directions and 16.3 km in the vertical direction. Vertical grid size varies from 100 m near the ground to 600 m near the top of the calculation domain.

Free-slip and adiabatic conditions are assumed at the top and bottom boundaries. Radiation conditions are assumed at the lateral open boundaries. Rayleigh damping with the e-folding time of 300 s is introduced above 12 km. Only the Kessler type warm rain process is considered in the cloud physics. The turbulent mixing is expressed by the 1.5-order closure scheme based on the prediction of turbulent kinetic energy. The Coriolis force is not included.

The vertical sounding data for the Del City storm used in Klemp and Wilhelmson (1978) is given for the horizontally uniform initial condition. In order to initiate convection, a thermal bubble is placed at 1.5 km AGL at the center of the calculation domain. The maximum temperature anomaly of the bubble is 4 K. In order to keep the storm in the calculation domain, the model coordinate system is translated eastward at 3.0 $ms^{-1}$and northward at 14.0 ms^{-1}. All the physical values hereafter shown are storm-relative.

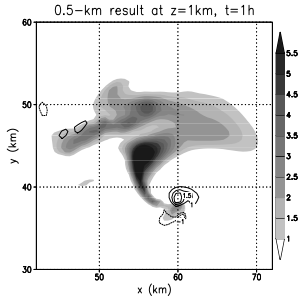

Fig.1: Horizontal cross section of rainwater (shade; g/kg) and vertical vorticity (contour; every 0.5×10^{-2} s^{-1}interval) for 0.5km-run at z=1km at 1 h.

* *Corresponding author address*:
Akira NODA, Dynamic Marine Meteorology Group, The Ocean Research Institute, University of Tokyo, 1-15-1, Minamidai, Nakano, Tokyo, 164-8639, Japan.
e-mail: noda@ori.u-tokyo.ac.jp

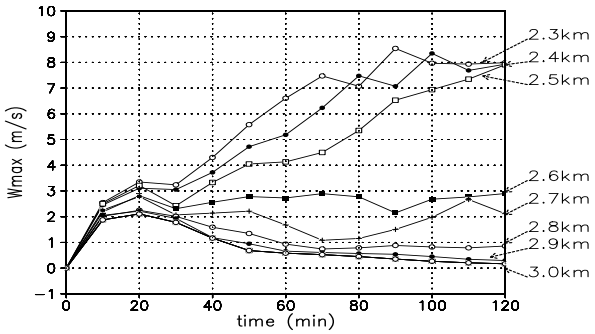

Fig.2: Time-evolution of the maximum vertical velocity at z=1km for 2.3km- $\sim$ 3.0km-runs.

3 RESULTS

3.1 0.5km-grid simulation

Since previous numerical studies on classic supercells have shown that the grid size of 0.5 km is enough to reproduce its characteristics (e.g., Klemp and Wilhelmson 1978; Adlerman et al. 1999), we regard the 0.5km-grid simulation as the standard run and it is used to compare with other results.

Figure 1 shows the horizontal cross section of the vertical vorticity and rainwater fields at z=1km at 1 h for 0.5-km run. As in the previous studies, the initial convection splits into left- and right-movers, and the right-mover develops more intensified than the left-mover does.

A region of the intense vertical vorticity called a mesocyclone develops in the right-mover. The intense airflow around the mesocyclone produces the hook-shaped rainwater pattern as in the previous studies.

3.2 Sensitivity experiments on the grid size

Figure 2 shows time-height cross sections of the maximum updraft at z=1km in the simulated storms for 2.3km- to 3.0km-runs. As the grid size is increased, the intensity of the updraft decreases, which is consistent with Weisman et al. (1997).

There are drastic changes in the evolution of the convective updraft between 2.5km- and 2.6km-runs and between 2.7km- and 2.8km-runs. When the grid size is larger than 2.6 km, the right-mover starts to be weakened after splitting of the storm while the left-mover continues to develop.

Figure 3 presents horizontal cross sections of the rainwater and vertical velocity at z=1 km at 90 min for 2.1km- $\sim$ 2.9km-runs. It is found that the convective clouds for the grid size of less than 2.5 km show supercellular characteristics (cf. Fig. 1). Those for the grid size larger than 2.5 km, however, do not exhibit such characteristics.

The figure also indicates that the convective clouds for the grid size of less than 2.7 km continue to develop during the simulation time of 3 h after the split of the initial convections triggered by the thermal bubble. When the grid size is greater than 2.8 km, however, the intensity of updraft weakens monotonically after the influence of the thermal bubble vanishes, and the cumulus convection eventually dissipates.

4 COMPARISON BETWEEN 2.5km- AND 2.6km-RUNS

In this section, we will focus on the right-movers for 2.5km- and 2.6km-runs and examine the reason why the convective cloud failed to evolve into a supercell in the latter.

Figure 4 indicates time evolution of the vertical velocity in the right-movers for 2.5km- and 2.6km-runs. The figure is constructed as follows: Firstly, the peak of the updraft is selected in the right-mover at z=1km. Then the intensities of updrafts are averaged horizontally over the selected point and its surrounding 4 grid points. This procedure is repeated every 600 s.

The updrafts of the right-movers in the two runs show similar evolution until 20 min. After 20 min, however, those convective clouds begin to evolve in a different manner. For example, the value of updraft in 2.6km-run begins to decrease while that in 2.5km-run increases. In order to understand the cause of this difference at 30 min, a momentum budget has been examined both for right-movers. The momentum equation under inviscid and Boussinesq approximation is written as

$$\frac{d\boldsymbol{v}}{dt} = -C_p\Theta\boldsymbol{\nabla}\pi + B\boldsymbol{k}, \qquad (1)$$

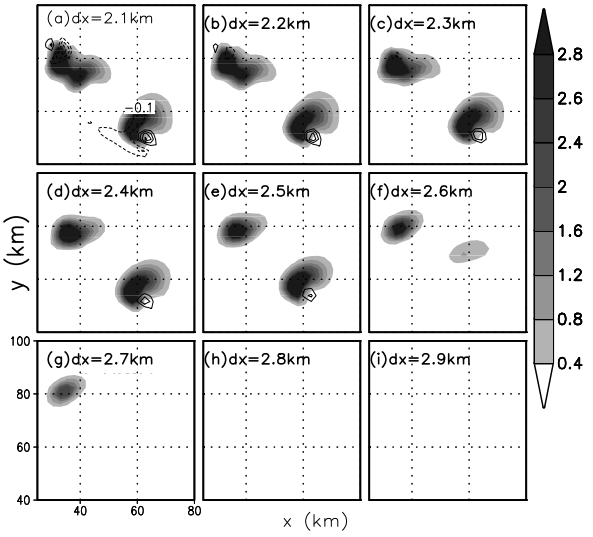

Fig.3: Horizontal cross sections of rainwater (shaded; g/kg) and vertical vorticity (contour; every 10^{-3}s^{-1} interval) fields at z=1km at 90 min for 2.1km- to 2.9km-runs.

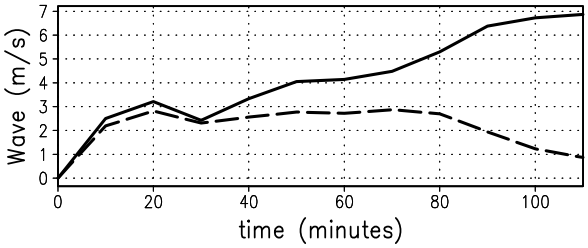

Fig.4: Time-evolutions of the spatially-averaged updraft intensities (ms^{-1}) at z=1km in the right-movers for 2.5km- (solid) and 2.6km- (dashed) runs.

where π is the Exner function, C_p (=1004 $m^2s^{-2}K^{-1}$) the specific heat of dry air at a constant pressure and Θ (=300 K) standard potential temperature.

Following the manner described in Rotunno and Klemp (1982), terms on the right-hand side of Eq. (1) can be grouped into two kinds of forces by decomposing π into π_d whose origin is the spatial variation of a wind field and π_b whose origin is the buoyancy. Note that an advection term of Eq. (1) is not shown in this paper because it does not play an essential role for evolution of the convective cloud. Eq. (1) becomes

$$\frac{d\boldsymbol{v}}{dt} = \underbrace{-C_p\Theta\boldsymbol{\nabla}\pi_d}_{F_d}\underbrace{-C_p\Theta\boldsymbol{\nabla}\pi_b + B\boldsymbol{k}}_{F_b}. \qquad (2)$$

The time evolutions of the vertical component of F_d, $F_b$and F_t(=F_d+ F_b) averaged over the five grid points at and around the grid point of the peak updraft are presented in Fig. 5.

Summation of F_d and $F_b$well explains the time-rate change of the updraft. For both runs, F_d contributes to the increase of the vertical velocity in the first 20 min. For 2.5km-run, F_d governs the evolution of the updraft over the 110 min shown in Fig. 5. For 2.6km-run, however, F_b is responsible for the time-rate change of the negative vertical velocity after 20 min. These results may be explained as follows: In order to maintain the convective cloud, it is necessary to lift the low-level air up to the level of free convection (LFC) by F_d because F_b is negative below this level. Once the low-level air is lifted to LFC by F_d, upward acceleration is maintained by F_b. However, if the lifting of the low-level air by F_d is once weakened, the low-level air cannot be lifted to LFC and the hydrometeors cannot be sustained by the updraft, which results in the decay of the convective cloud.

In order to further examine the cause for the maintenance of the upward acceleration due to F_d associated with the mesocyclone aloft in detail, the vorticity budget is examined. A vertical component of the vorticity equation for an inviscid fluid is

$$\frac{d\zeta}{dt} = \xi\frac{\partial w}{\partial x} + \eta\frac{\partial w}{\partial y} + \zeta\frac{\partial w}{\partial z}, \qquad (3)$$

where ξ, η and ζ denotes the x-, y- and z-component of the vorticity vector, respectively. The first and second terms on RHS are called tilting term, and the third stretching term.

Time-rate change of the vertical vorticity, tilting term and magnitude of the horizontal vorticity are shown in Fig. 6. The values in the figure are again averaged over five grid points. In both 2.5km- and 2.6km-runs, time-rate change of the vertical vorticity lags that of the updraft, suggesting that the upward pressure gradient force caused by the mesocyclone aloft contributes to the upward acceleration of the vertical velocity at z=1 km as shown in Fig. 5 of F_d.

The time change of the vertical vorticity for 2.5km-run indicates similar to that for 2.5km-run in the first 30 min. After 30 min, however, the growth of the vertical vorticity for 2.6km-run stops at 7.5 $\times 10^{-4}$ s^{-1}, while that for 2.5km-run exceeds over at that of 9.5 $\times 10^{-4}$ s^{-1}. We can see that the original source of the vertical vorticity is tilting of the horizontal vorticity in Eq. (3).

Next, the cause for the tilting term is examined. The tilting terms show similar time-rate change to the vertical vorticity in both results. On the other hand, the magnitude of horizontal vorticity does not show such time-rate change , suggesting that a cause for the difference of tilting terms in both results lies in the difference in the horizontal gradient of the vertical velocity.

It can be said that the difference of the tilting terms occurs because the horizontal vorticity is almost determined by the vertical wind shear in the basic field. Therefore, difference of time-rate changes of the tilting term mostly depends on the horizontal gradient of the vertical velocity.

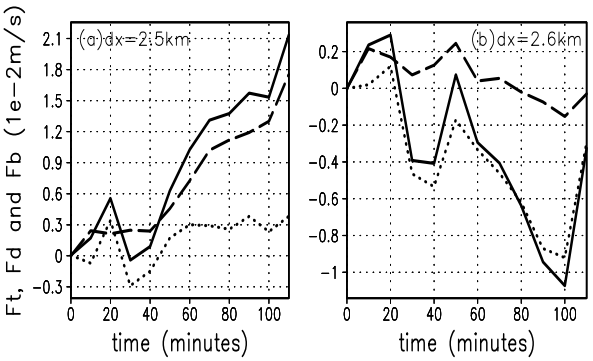

Fig.5: Time-evolutions of the vertical components of spatially-averaged F_t(solid), F_d(dashed) and F_b(dotted) at z=1km for (a)2.5km- and (b)2.6km-runs. Unit of the vertical axis is 10^{-2} ms^{-2}

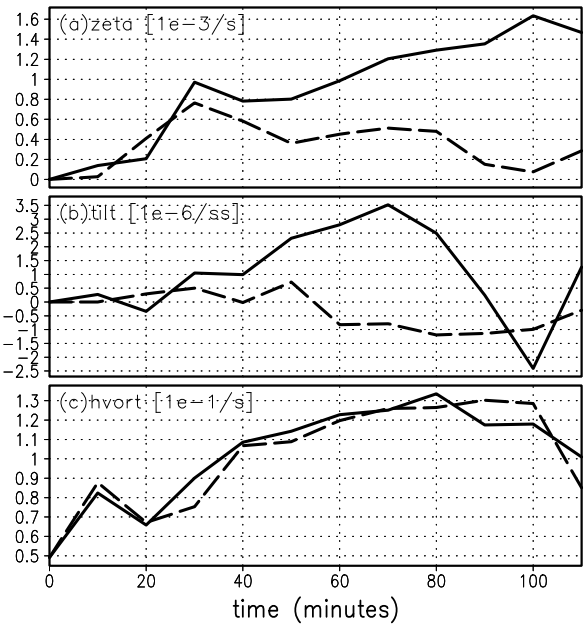

Fig.6: Time-evolution of spatially-averaged (a)ζ ($10^{-3}s^{-1}$), (b) tilting term ($10^{-6}s^{-2}$) and (c) magnitude of horizontal vorticity ($10^{-1}s^{-1}$) at z=1km for 2.5km- (solid) and 2.6km- (dashed) runs.

The horizontal gradient of the vertical velocity becomes, even if intensity of vertical velocity is almost the same, smaller in a result at larger grid size. Therefore, the generation of the vertical vorticity due to tilting of the horizontal vorticity becomes smaller in 2.6km-run. Thus, the vertical vorticity of the mesocyclone would not reach the intensity strong enough to lift the low-level negative buoyant air up to LFC.

5 CONCLUDING REMARKS

Dependence of a classic supercell storm on grid size has been examined. It is found that there are two values of the grid size across which the storm behavior changes drastically. One is between 2.5 km and 2.6 km, and the other between 2.7 km and 2.8 km.

The initial storm evolves into a supercell after splitting when grid size is less than 2.5 km. When the grid size is greater than 2.6 km, the split storms do not show supercellular characteristics. In particular, the split storm that would be expected to become a right-mover eventually dissipates. The reason why the storm for 2.6km-run fails to evolve to the supercell is that the dynamic pressure gradient force due to the mesocyclone aloft is not sufficient to lift the low-level negatively-buoyant air up to LFC. When the grid size is greater than 2.7 km, the long lasting nature of a storm is not realized anymore. A reason of this variation is not clear.

The present paper has demonstrated that a time-change of the grid size by 100 m could cause not only quantitative but also qualitative change of behavior of the convective storm. The critical grid sizes at which the storm behavior changes drastically are likely to vary from model to model: It would depend on a dynamic frame, cloud physics parameterization, turbulence parameterization, environmental condition and so on. It could also depend on the type of storms. However, it is nearly certain that any mesoscale model could have a critical grid size across which the storm behavior changes drastically. If this is the case, one has to be careful in choosing the grid size when one attempts to predict individual storms or meso β-scale precipitation system in which individual convection cells play an important role in maintaining the parent system.

ACKNOWLEDGMENTS

The present work is partly supported by Grant-in-Aids for Scientific Research on Priority Areas (B)(2) No.1212520, the Ministry of Education, Culture, Sports, Science, and Technology. This simulation was made using the Advanced Regional Prediction System(ARPS) developed by the Center for Analysis and Prediction of Storms (CAPS), University of Oklahoma. CAPS is supported by the National Science Foundation and the Federal Aviation Administration through combined grant ATM92-20009.

REFERENCES

Adlerman, E. J., K. K. Droegemeier, and R. P. Davis-Jones, 1999: A numerical simulation of cyclic mesocyclogenesis. *J. Atmos. Sci.*, **56**, 2045-2068.

Adlerman, E. J., and K. K. Droegemeier, 2001: The sensitivity of numerically simulated cyclic mesocyclogenesis to variations in model physical and computational parameters. Submitted to *Mon. Wea. Rev.*

Yanase, W., H. Niino, and K. Saito, 2001: Cloud-resolving numerical simulation of a polar low over the Japan sea. Preprints, *9th Conf. on Mesoscale Processes*, Ft. Lauderdale, Florida, Amer. Meteor. Soc., 497-501.

Klemp, J. B., and R. B. Wilhelmson, 1978: The simulation of three-dimensional convective storm dynamics. *J. Atmos. Sci.*, **35**, 1070-1096.

Rotunno, R., and J. B. Klemp, 1982: The influence of the shear-induced pressure gradient on thunderstorm motion. *Mon. Wea. Rev.*, **110**, 136-151.

Weisman, M. L., W. C. Skamarock, and J. B. Klemp, 1997: The resolution dependence of explicitly modeled convective systems. *Mon. Wea. Rev.*, **125**, 527-548.

Xue, M., K. K. Droegemeier, V. Wong, A. Shapiro, and K. Brewster, 1995: *ARPS Version 4.0 User's Guide.* The Center for Analysis and Prediction of Storms, University of Oklahoma, 380 pp.